Title

N-Methyl-N-nitrosourea Induced 3-Glutathionylated DNA-Cleavage Products in Mammalian Cells.

Journal

Analytical Chemistry, 94(45)

Authors

Yin, Jiekai

Gates, Kent

Wang, Yinsheng

Publication Date

2022-11-15

DOI

10.1021/acs.analchem.2c02003

Peer reviewed

HHS Public Access

Author manuscript

Anal Chem. Author manuscript; available in PMC 2023 November 15.

Published in final edited form as:

Anal Chem. 2022 November 15; 94(45): 15595–15603. doi:10.1021/acs.analchem.2c02003.

N-Methyl-*N*-nitrosourea Induced 3′-Glutathionylated DNA-Cleavage Products in Mammalian Cells

Jiekai Yin,

Environmental Toxicology Graduate Program, University of California, Riverside, California 92521-0403, United States

Kent S. Gates,

Department of Chemistry, University of Missouri, Columbia, Missouri 65211, United States; Department of Biochemistry, University of Missouri, Columbia, Missouri 65211, United States

Yinsheng Wang

Environmental Toxicology Graduate Program and Department of Chemistry, University of California, Riverside, California 92521-0403, United States

Abstract

Apurinic/apyrimidinic (AP) sites, that is, abasic sites, are among the most frequently induced DNA lesions. Spontaneous or DNA glycosylase-mediated β-elimination of the 3′-phosphoryl group can lead to strand cleavages at AP sites to yield a highly reactive, electrophilic 3′-phospho-α,β-unsaturated aldehyde (3′-PUA) remnant. The latter can react with amine or thiol groups of biological small molecules, DNA, and proteins to yield various damaged 3′-end products. Considering its high intracellular concentration, glutathione (GSH) may conjugate with 3′-PUA to yield 3-glutathionyl-2,3-dideoxyribose (GS-ddR), which may constitute a significant, yet previously unrecognized endogenous lesion. Here, we developed a liquid chromatography tandem mass spectroscopy method, in combination with the use of a stable isotope-labeled internal standard, to quantify GS-ddR in genomic DNA of cultured human cells. Our results revealed the presence of GS-ddR in the DNA of untreated cells, and its level was augmented in cells upon exposure to an alkylating agent, *N*-methyl-*N*-nitrosourea (MNU). In addition, inhibition of AP endonuclease (APE1) led to an elevated level of GS-ddR in the DNA of MNU-treated cells. Together, we reported here, for the first time, the presence of appreciable levels of GS-ddR in cellular DNA, the induction of GS-ddR by a DNA alkylating agent, and the role of APE1 in modulating its level in human cells.

Graphical Abstract

Corresponding Author: **Yinsheng Wang** – Environmental Toxicology Graduate Program and Department of Chemistry, University of California, Riverside, California 92521-0403, United States; Phone: (951)827-2700; yinsheng.wang@ucr.edu.

Supporting Information

The Supporting Information is available free of charge at https://pubs.acs.org/doi/10.1021/acs.analchem.2c02003.

Supplementary experimental conditions; ESI-MS and MS/MS of purified GS-ddR-containing oligodeoxynucleotides; LC–MS/MS results; and calibration curves (PDF)

Complete contact information is available at: https://pubs.acs.org/10.1021/acs.analchem.2c02003

The authors declare no competing financial interest.

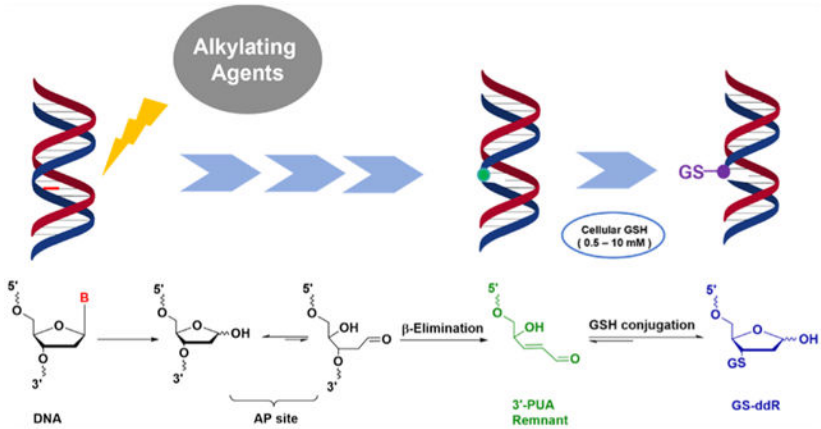

INTRODUCTION

Apurinic/apyrimidinic (AP) sites, or abasic sites, are one of the most abundant endogenous DNA lesions. Both endogenous and environmental sources,[1–9] for example, spontaneous depurination, reactive oxygen species, and alkylating agents, can lead to the formation of AP sites directly.[10,11] AP sites can also be produced via DNA glycosylase-mediated removal of damaged nucleobases induced by these processes.[12–14] If not efficiently repaired, AP sites may block DNA replication and cause mutagenesis.[15–17] Moreover, spontaneous and DNA glycosylase-catalyzed β-elimination of the phosphoryl group on the 3′ side of AP sites can lead to DNA strand cleavage and generate an electrophilic 3′-phospho-α,β-unsaturated aldehyde (3′-PUA) (Scheme 1),[18–20] whose existence in mammalian cells has been confirmed.[21] 3′-PUA is more reactive and toxic than AP sites,[22] and it brings additional complexity to the damage products derived from AP sites,[23] including the conjugate addition adducts with thiols,[24–26] DNA DNA interstrand cross-links,[27–31] and DNA-protein cross-links.[32–36] The formation rate of cellular 3′-PUA is further elevated in the presence of endogenous low-molecular-weight polyamines (e.g., spermine)[37,38] or from the action of bifunctional DNA glycosylases.[13,39,40]

Alkylating agents can damage nucleobases in DNA directly or following metabolic activation.[41–43] Despite their cytotoxic and mutagenic effects, some alkylating agents are widely used in cancer chemotherapy.[43,44] *N*-Methyl-*N*-nitrosourea (MNU) is a prototypical S_N1-type methylating agent that modifies DNA in a similar way as temozolomide, a widely used cancer chemotherapeutic agent (Scheme 2).[45,46] These agents can methylate ring nitrogen and exocyclic oxygen atoms of nucleosides, where the major DNA adducts include *N*7-methyl-2′-deoxyguanosine (*N*7-MedG) and O^6-methyl-2′-deoxyguanosine (O^6-MedG). Mispairing during DNA replication renders O^6-MedG cytotoxic and mutagenic.[47–49] O^6-MedG is repaired by O^6-methylguanine-DNA methyltransferase (MGMT), nucleotide excision repair (NER), or mismatch repair (MMR).[42,43,46] The cationic *N*7-MedG is removed through depurination[50] or base excision repair (BER). Spontaneous depurination of some alkylated DNA lesions and DNA glycosylase-mediated elimination of alkylated nucleobases can result in elevated levels of AP sites in cells, along with accompanying increases in 3′-PUA.

3′-PUA exhibits high reactivity with thiol, and we recently reported the formation of the 3′-glutathionylated DNA strand-cleavage product, that is, 3′-glutathionyl-2,3-dideoxyribose (GS-ddR), in synthetic duplex DNA in vitro (Scheme 1).[51] Considering that the cellular concentration of GSH ranges from 0.5 to 10 mM,[52,53] we reason that the same product may form in cellular DNA. Here, we developed a stable-isotope-dilution-based liquid chromatography tandem mass spectroscopy (LC–MS/MS) method for the quantification of the basal level and MNU-induced formation of GS-ddR in cultured human cells.

EXPERIMENTAL SECTION

GS-ddR-Containing ODN Generation.

One nmol of 2′-deoxyuridine (dU)-containing ODN, 5′-ACATGAACUTA-GACATATACA-3′, was incubated with 5 U of uracil DNA glycosylase (UDG) at 37 °C for 1 h in 10 μL of UDG reaction buffer. Spermine was subsequently introduced at a final concentration of 10 mM, and water was added to make the total volume 20 μL. The mixture was incubated at 37 °C for 30 min to generate the amine-mediated strand cleavage via β-elimination. To the mixture was subsequently added GSH (10 mM), and the mixture was incubated at 37 °C overnight to yield the GS-ddR end group. Finally, GS-ddR-MX-containing ODN was obtained by treating with methoxyamine (MX, 10 mM) at 37 °C for 1 h to stabilize the aldehyde group of GS-ddR. The products were confirmed by electrospray ionization MS (ESI-MS) and MS/MS characterizations. The [$^{13}C_2$, ^{15}N]-GS-ddR-MX-containing ODN was generated using similar procedures except that GSH in the above procedures was replaced with [$^{13}C_2$, ^{15}N]-GSH. The resulting GS-ddR-MX-containing ODNs were purified by high-performance liquid chromatography (HPLC) (Supplementary Experimental Section), confirmed by ESI-MS and MS/MS analyses, and quantified by UV absorbance at 260 nm.

Characterization of GS-ddR-MX Monophosphate by LC–MS/MS.

GS-ddR-MX-containing ODN (50 pmol) or genomic DNA extracted from HEK293T cells (10 μg) was incubated with 1 unit of nuclease P1 in a 20 μL solution containing 30 mM sodium acetate (pH 5.6) and 10 mM $ZnCl_2$ at 37 °C overnight to generate the GS-ddR-MX mono-phosphate. After the removal of enzymes in the digestion mixture with chloroform extraction, the resulting aqueous layer was dried by Speed-Vac and the dried residue was dissolved in doubly distilled water. The GS-ddR-MX monophosphate (5 pmol) or digested nucleotide (5 μg) mixture was subjected to LC–MS/MS analysis on an LTQ linear ion-trap mass spectrometer (Thermo Fisher Scientific, San Jose, CA) equipped with an Agilent 1200 capillary HPLC (Agilent Technologies, Santa Clara, CA). A 0.5 × 250 mm Zorbax SB-C18 column (5 μm particle size, Agilent Technologies, Santa Clara, CA) was used for the LC separation at a flow rate of 8.0 μL/min. Mobile phases were 400 mM 1,1,1,3,3,3-hexafluoro-2-propanol (pH was adjusted to 7.0 with triethylamine) in water (solution A) and methanol (solution B). A gradient of 5% B for 5 min, 5–70% B in 25 min, 70–90% B in 1 min, and 90% B for 10 min was employed. The mass spectrometer was operated in the negative-ion mode, where the MS/MS results for the $[M–H]^-$ ions of GS-ddR-MX monophosphate (m/z 531) and [$^{13}C_2$, ^{15}N]-GS-ddR-MX monophosphate (m/z 534) were acquired (Figure 2).

ODN Release Efficiency Test.

For constructing the calibration curves of GS-ddR, different amounts of GS-ddR-MX-containing ODN were mixed individually with a fixed amount (20 fmol) of the stable isotope-labeled ODN together with 20 μg of calf thymus DNA. In this vein, calf thymus DNA was confirmed to be free of GS-ddR based on LC–MS/MS analysis. The mixtures were subsequently digested with enzymes, enriched by off-line HPLC, and subjected to LC–MS/MS analyses. Calibration curves were generated by plotting the ratios of peak areas found in the selected-ion chromatograms (SICs) for monitoring the transitions of GS-ddR-MX and [$^{13}C_2$, ^{15}N]-GS-ddR-MX versus their spike-in molar ratios.

For analyzing the quantification accuracy of the LC–MS/MS method, calf thymus DNA (20 μg) was spiked with different amounts of GS-ddR-MX-containing ODN until its final levels reached 0, 0.06, 0.3, 0.6, 1.2, 3, 6, and 12 lesions per 10^6 nucleosides. [$^{13}C_2$, ^{15}N]-GS-ddR-MX-containing ODN (20 fmol) was added to each sample. The DNA was subsequently digested by enzymes, enriched by off-line HPLC, and subjected to LC–MS/MS analyses. Recovery calibration curves were constructed by plotting the detected levels of GS-ddR in calf thymus DNA versus the level of spiked-in GS-ddR-containing ODN.

Genomic DNA Extraction and Methoxyamine Derivatization.

Total genomic DNA was extracted from MNU-treated or control untreated cells based on a previously published high-salt method[54] with some modifications. In this vein, several different conditions were employed: a lysis buffer (80 μL) containing 20 mM Tris (pH 8.1), 20 mM ethylenediamine tetraacetic acid (EDTA), 400 mM NaCl, 1% sodium dodecyl sulfate (SDS), and 5.0 mM methoxyamine, together with 20 μL of proteinase K (20 mg/mL), was added to an Eppendorf tube containing pellets of cells harvested from one T25 flask and incubated in a water bath at 55 °C for 1, 2, 4, 6, 16, and 24 h to examine the effects of lysis time on the levels of measured GS-ddR. The DNA samples from the subsequent dose-dependent MNU treatment experiments were obtained by employing these conditions with a lysis time of 16 h.

We also changed the concentrations of methoxyamine to 1.0 and 10.0 mM and found that 5.0 mM of methoxyamine yielded the most reproducible results in GS-ddR measurement. In addition, we conducted the cell lysis at 37 °C for 2 and 16 h; however, we were not able to obtain adequate amount of DNA for the subsequent LC–MS/MS analysis, suggesting that proteinase K digestion at 37 °C is insufficient to release genomic DNA from its bound histones and other proteins.

Further optimization was conducted to improve the DNA yields. In particular, cells from one T25 flask were resuspended with 200 μL of lysis buffer containing 20 mM Tris (pH 8.1), 20 mM EDTA, 400 mM NaCl, and 5.0 mM methoxyamine and mixed by pipetting. Twenty-five microliters of proteinase K solution (20 mg/mL) were subsequently added to the mixtures, and the samples were mixed by vortexing. To the mixture was then added 25 μL of 10% SDS. The sample tubes were inverted several times, placed on a thermal mixer, and then incubated at 55 °C and at a rotating speed of 900 rpm. After a 16 h incubation, 125 μL of saturated NaCl solution (0.5 volume) was added to the mixture and mixed by

vortexing for 1 min followed by another 15 min incubation at 55 °C. The resulting mixture was centrifuged at 13,000 rpm for 30 min at 4 °C. The supernatant was transferred to a fresh tube and mixed with 2 volumes of cold ethanol to precipitate the nucleic acid. The DNA samples from time-dependent MNU treatment were obtained by employing these optimized cell lysis conditions.

The nucleic acid pellet was washed once with 70% ethanol and dissolved in 94 μL of doubly distilled water. Five microliters of RNase A (10 mg/mL) and one microliter of RNase T1 (100 units/μL) were added to digest the RNA in the nucleic acid mixture. After an overnight incubation at 37 °C, the enzymes were removed by extraction with a half volume of chloroform/isoamyl alcohol (24:1, v/v). The genomic DNA was then precipitated from the aqueous layer with 2 volumes of ethanol. DNA pellets were washed with 70% cold ethanol, allowed to air-dry at room temperature, redissolved in doubly distilled water, and quantified by nanodrop.

Enzymatic Digestion of Genomic DNA.

The DNA sample (20 μg) from control or MNU- and/or APE inhibitor-treated HEK293T cells was digested with 2 unit of nuclease P1 in a 45 μL buffer containing 30 mM sodium acetate (pH 5.6) and 10 mM $ZnCl_2$ at 37 °C for 4 h. [$^{13}C_2$, ^{15}N]-GS-ddR-MX-containing ODN (20 fmol) was added to the mixture to serve as an internal standard for the quantification of GS-ddR. To the mixtures were then added 5 unit of alkaline phosphatase and 6 μL of 0.5 M Tris–HCl (pH 8.9) and doubly distilled water to render the total volume 60 μL. After incubation at 37 °C for 2 h, the enzymes in the digestion mixture were removed by extraction with 0.5 volume of chloroform. The aqueous layer was dried by Speed-Vac and reconstituted in 100 μL of water for off-line HPLC enrichment.

Off-Line HPLC Enrichment.

The HPLC separation was performed on a Beckman HPLC system with pump module 125 and UV detector module 126. An Hypersil BDS C18 column (4.6 × 250 mm, 5 μm in particle size, 130 Å in pore size, Thermo Fisher Scientific, San Jose, CA) was employed for the enrichment of GS-ddR-MX and O^6-MedG from the enzymatic digestion mixture. A solution of 10 mM ammonium formate in water (solution A) and a mixture of solution A and acetonitrile (70/30, v/v) (solution B) were used as mobile phases, and a gradient composed of 0–20% B in 30 min, 20–100% B in 10 min, and 100% B for 5 min was employed with a flow rate of 0.8 mL/min. The HPLC fractions in the retention time range of 12–14 min were pooled for GS-ddR-MX, and those fractions in 34–38 min were combined for O^6-MedG (Figure 3B). The eluents were dried in a Speed-Vac, reconstituted in doubly distilled water, and subjected to nLC-nESI-MS/MS analysis. Modified nucleosides were not detected in the fractions collected from the blank injection between samples, indicating that there is no analyte carry-over during the enrichment.

nLC-nESI-MS/MS Quantification of GS-ddR and O^6-MedG.

nLC-nESI-MS/MS analyses of GS-ddR and O^6-MedG were conducted on an LTQ-XL linear ion trap mass spectrometer equipped with a nano-ESI source and coupled with an EASY-nLC II system or on a Q Exactive Plus quadrupole-Orbitrap mass spectrometer equipped

with a Nanospray Flex source and coupled with a Dionex UltiMate 3000 RSLCnano UPLC system (Thermo Fisher Scientific, San Jose, CA).

For the analyses on an LTQ-XL linear ion trap mass spectrometer coupled with an EASY-nLC II system, the nucleoside mixture was first loaded onto a trapping column (150 μm × 40 mm) at a flow rate of 2.5 μL/min within 7 min. The nucleosides were then eluted onto an analytical column (75 μm × 200 mm) at a flow rate of 300 nL/min. Both trapping and analytical columns were packed in-house with Magic C18 AQ (5 μm in particle size, 200 Å in pore size, Michrom BioResource, Auburn, CA). Formic acid (0.1%, v/v) in water and acetonitrile were used as solution A and solution B, respectively. A gradient of 0–50% B in 30 min, 50–90% B in 1 min, and 90% B for 5 min was employed. The LTQ-XL linear ion trap mass spectrometer was operated in the positive-ion mode. The voltage for electrospray was 2.0 kV, and the temperature for the ion transfer tube was 275 °C. The capillary and tube lens voltages were 45 and 73 V, respectively. Automated gain control values were set at 3×10^4 and 1×10^4 for MS and MS^n, respectively. In MS/MS analysis of GS-ddR-MX, the isolation width for precursor ion selection was 3 *m*/*z* unit, the normalized collision energy was 35%, the activation Q was 0.3, and the activation time was 30 ms. In the MS/MS/MS analysis of O^6-MedG, the isolation widths, normalized collision energies, and the activation times were set as 3 and 2 *m*/*z* units, 35 and 38%, and 30 and 50 ms for MS^2 and MS^3, respectively. The activation Q was 0.3 for both MS^2 and MS^3. MS/MS results for the $[M + H]^+$ ions of GS-ddR-MX (*m*/*z* 453) and [$^{13}C_2$, ^{15}N]-GS-ddR-MX (*m*/*z* 456) were acquired, and MS/MS/MS results arising from the further cleavage of the $[M + H]^+$ ions of the nucleobase portions of O^6-MedG (*m*/*z* 166) and D_3-O^6-MedG (*m*/*z* 169) were recorded (Figures S4–S6).

For the analyses on the Q Exactive Plus quadrupole-Orbitrap mass spectrometer coupled with a Dionex UltiMate 3000 RSLCnano UPLC system, a trapping column (150 μm × 40 mm) and an analytical column (75 μm × 200 mm) packed with Magic C18 AQ (5 μm in particle size, 200 Å in pore size, Michrom BioResource, Auburn, CA) were utilized. Formic acid (0.1%, v/v) in water and formic acid (0.1%, v/v) in acetonitrile/H_2O (4:1, v/v) were used as mobile phases A and B, respectively. A gradient of 0–50% B in 20 min, 50–90% B in 1 min, and 90% B for 5 min was employed at a flow rate of 300 nL/min. The Q Exactive Plus quadrupole-Orbitrap mass spectrometer was operated in the positive-ion mode. The voltage for electrospray was 2.0 kV and the capillary temperature was 275 °C. The precursor ions were isolated in the quadrupole at an isolation window of 3.0 *m*/*z* and fragmented in an HCD collision cell at a normalized collision energy of 35. The MS/MS resolution was 70,000, the automated gain control target was 1×10^5, and the maximum accumulation time was 100 ms. MS/MS results for the $[M + H]^+$ ions of GS-ddR-MX (*m*/*z* 453.2) and [$^{13}C_2$, ^{15}N]-GS-ddR-MX (*m*/*z* 456.2) were acquired (Figures S7 and S8).

The numbers of moles of GS-ddR-MX and O^6-MedG in each sample were calculated from the peak area ratios of the unlabeled analytes to the corresponding stable isotope-labeled standards, the calibration curves, and the amounts of stable isotope-labeled standards added. The levels of GS-ddR-MX and O^6-MedG were expressed as the number of lesions per 10^6 deoxynucleosides.

RESULTS AND DISCUSSION

Preparation and LC–MS and MS/MS Characterizations of a GS-ddR-Containing ODN.

Because of the reactivity of the 3′-terminal aldehyde, a complex mixture of products can form from strand cleavage sites in DNA.[23] Previous studies showed that methoxyamine (MX) is capable of blocking AP sites and interfering with the enzymatic activity of AP-endonuclease (APE1) during BER; this property of MX renders it a sensitizing agent in combination chemotherapy to enhance the cytotoxic effects of alkylating agents such as temozolomide.[55–57] In this study, we employed MX to cap and stabilize GS-ddR, which leads to the formation of a stable oxime derivative[58–60] (Figure 1A).

To generate GS-ddR-containing ODN, we first treated a single-stranded uracil-containing ODN with uracil-DNA glycosylase (UDG) to generate the AP site.[30] We also added spermine to the reaction mixture to promote the strand cleavage at the AP site.[37] The resulting 3′-PUA-containing ODN was incubated sequentially with GSH and MX to generate the GS-ddR-MX (Figure 1B). LC–MS/MS analysis of the GS-ddR-containing ODN confirmed the sequence of the ODN and the presence of GS-ddR-MX at its 3′-terminus (Figure S1). We also replaced GSH with [$^{13}C_2$, ^{15}N]-GSH to generate the stable-isotope-labeled GS-ddR-containing ODN (Figure 1C). The ODN was further purified by HPLC and characterized by ESI-MS and MS/MS (Figure S2).

To validate the structure of GS-ddR, we digested the GS-ddR-containing ODN with nuclease P1 to yield nucleoside-5′-monophosphates and subjected the products to LC–MS/MS analysis on an LTQ linear ion-trap mass spectrometer. Upon collision-induced dissociation, a number of product ions are formed from the $[M - H]^-$ ion (m/z 531) of GS-ddR-MX monophosphate (Figure 2B), where the observed fragment ions in the MS/MS are consistent with its structure (Figure 2C). Similar retention time and fragment ions were observed for the $[M - H]^-$ ion of [$^{13}C_2$, ^{15}N]-GS-ddR-MX monophosphate (Figure 2). The product ions of m/z 306 and 309, which arise from the neutral loss of the MX-bound 2-deoxyribose monophosphate, were employed for monitoring GS-ddR-MX and [$^{13}C_2$, ^{15}N]-GS-ddR-MX monophosphates, respectively.

Development of an LC–MS/MS Method for the Quantification of GS-ddR in DNA.

GS-ddR can form from the strand cleavage at AP sites in DNA. We reason that the MNU-induced generation of AP sites in mammalian cells[61] could give rise to augmented formation of GS-ddR. Indeed, we were able to detect GS-ddR-MX monophosphate in the nuclease P1 digestion mixture of DNA samples isolated from MNU-treated HEK293T cells with majority of the product ions in the MS/MS matching with those of the GS-ddR-MX monophosphate standard. Weak signals for GS-ddR-MX monophosphate were also detected in the DNA sample isolated from the control untreated HEK293T cells (Figure S3). However, the signal intensity of GS-ddR-MX in genomic DNA samples was quite low, indicating that the LC–MS/MS method requires further optimization for the reliable and accurate quantification of GS-ddR.

Considering that GS-ddR-MX may possess a better ionization efficiency in the positive-ion mode than GS-ddR-MX monophosphate in the negative-ion mode, we added

alkaline phosphatase to the nuclease P1 digestion mixture to convert the GS-ddR-MX monophosphate to GS-ddR-MX. The steady-state levels of AP sites and 3′-PUA within mammalian cells were reported to be approximately 1 lesion per 10^6 nucleosides or lower.[21,62] Thus, GS-ddR may also be present at a relatively low level. To enable its robust detection, we employed off-line HPLC enrichment to remove canonical nucleosides and buffer salts in the enzymatic digestion mixture, which provides cleaner sample matrices and better facilitates the detection of GS-ddR.[63] In this vein, GS-ddR-MX eluted immediately after 2′-deoxycytidine (dC) and a 2 min collection window allows for full capture of GS-ddR-MX from the digestion mixture (Figure 3B). We employed LC-nESI-MS/MS on a linear ion-trap mass spectrometer to characterize GS-ddR-MX. The fragment ions observed in MS/MS are consistent with the structure of GS-ddR-MX. The most abundant product ion at m/z 277 and 280 were employed for subsequent monitoring of GS-ddR-MX and [$^{13}C_2$, ^{15}N]-GS-ddR-MX, respectively (Figure S4).

We next assessed the recovery of GS-ddR-MX during the workflow of enzymatic digestion, off-line HPLC enrichment, and LC–MS/MS analysis by employing the aforementioned GS-ddR-MX-containing ODNs. Briefly, we spiked 20 μg of calf thymus DNA with increasing amounts of unlabeled-GS-ddR-MX-containing ODN along with a fixed amount (20 fmol) of [$^{13}C_2$, ^{15}N]-GS-ddR-MX-containing ODN, which served as an internal standard (Figure 3A). We plotted the detected vs spiked-in levels of GS-ddR in calf thymus DNA, and linear regression analysis of the data yielded a slope of 0.9922 and an R^2 value of 0.9977 (Figure 3C), suggesting the robustness of the analytical workflow in measuring GS-ddR. In this vein, using stable-isotope-labeled ODN as the internal standard can also account for potential incomplete release of the lesion from DNA during enzymatic digestion, thereby allowing for accurate measurement of the level of GS-ddR in cellular DNA.

Quantification of MNU-Induced GS-ddR in Mammalian Cells.

We next applied the above-described LC–MS/MS method to assess the formation of GS-ddR in MNU-treated HEK293T cells. By the virtue of using MX as a derivatization agent for GS-ddR, we added MX to the lysis buffer during our DNA extraction procedure and optimized the concentration of MX. Our results showed that MNU treatment led to substantial elevations in the levels of GS-ddR in DNA of HEK293T cells. Compared with the levels of GS-ddR detected in DNA extracted with the presence of 1 or 10 mM MX in the lysis buffer, inclusion of 5 mM MX in the lysis buffer provided more reproducible results (Figure S9a). In addition, the levels of GS-ddR in DNA isolated from HEK293T cells were very similar when 5 or 10 mM MX was added during the cell lysis step, indicating that the derivatization was complete with 5 mM MX (Figure S9a). Hence, we employed 5 mM MX for the subsequent experiments. It is of note that the detected levels of the GS-ddR were lower with 5 or 10 mM of MX than with 1 mM of MX. The exact reason is unclear, although we speculate that higher concentrations of MX may allow for more effective trapping of the AP site, thereby preventing artificial formation of GS-ddR from AP sites during the cell lysis step.

Unavoidable generation of AP sites and strand breaks during sample workup has the potential to induce GS-ddR. In this regard, even though it was reported that the rate of

N-glycosidic bond hydrolysis and AP site formation (0.64 per 10^7 dN per h at 37 °C and pH 7.4) is quite slow at near-neutral pH,[62,64] the sample preparation workflow, especially the cell lysis step, may still introduce artifacts to GS-ddR measurements. Thus, we monitored the formation of GS-ddR during the course of cell lysis to identify conditions that minimize artifacts, following a similar method described previously for AP site measurement.[62] We observed that there is a lysis time-dependent increase in the level of measured GS-ddR in genomic DNA isolated from HEK293T cells during the first 16-h of cell lysis, which is accompanied with a sharp increase in the level of GS-ddR from 16 to 24 h (Figure S9b). The time-dependent increase in the level of GS-ddR may arise from the release of GS-ddR from histone and other proteins after their proteolysis, although artificial generation of GS-ddR from spontaneous depurination and/or from conjugation of GSH with existing AP sites during lysis may also contribute, in part, to the lysis time-dependent increase in the level of GS-ddR. Considering that the time-dependent increase in the level of GS-ddR was relatively small in the initial 16 h and high yield of DNA was obtained with a 16 h incubation with proteinase K, we employed a 16 h incubation time for cell lysis and GS-ddR derivatization during DNA isolation for the subsequent experiments.

It is worth noting that the level of GS-ddR (0.2–0.5 lesions per 10^6 nucleosides with a 16 h lysis time, Figures S9b and 4A) was slightly lower than the previously reported levels of AP sites and 3′-PUA, which were approximately 1 lesion per 10^6 nucleosides or lower.[21,62] This finding is consistent with the fact that GS-ddR arises from AP sites and 3′-PUA, and the formation of GS-ddR is in competition with the formation of other AP site derivatives, for example, DNA–DNA interstrand cross-links and DNA-protein cross-links.

We next investigated how treatment with different doses of MNU modulates the formation of GS-ddR in HEK293T cells. For comparison, the levels of O^6-MedG were also measured in the same DNA samples using a previously reported method.[65] We treated HEK293T cells with 50, 100, 200, 500 μM, and 1 mM of MNU for 1 h and then measured the levels of these two lesions in cellular DNA. Our results revealed dose-dependent induction of GS-ddR and O^6-MedG (Figure 4A,B).

We next treated HEK293T cells with 100 μM and 1 mM of MNU for 0, 1, 8, and 24 h and then measured the levels of these two lesions in cellular DNA, where MNU treatment with 0 h was considered as the control group. Our results showed that upon treatment with 100 μM MNU, the levels of GS-ddR increased during the initial 8 h and then decreased at 24 h; while treatment with 1 mM MNU also results in a progressive increase of GS-ddR initially, it reached a plateau after 8 h (Figure 4C). This might be attributed to the diminished repair of GS-ddR in cells exposed with a toxic concentration of MNU (1 mM), where our cell survival assay results showed a 20% reduction in cell survival after a 1 h exposure with 1 mM MNU (Figure S11). A comparison of the time-dependent change in the levels of the two lesions showed that, upon treatment with 100 μM MNU, the level of O^6-MedG started to decrease from 1 to 8 h, whereas that of GS-ddR began to decrease from 8 to 24 h (Figure 4D). This result is consistent with the notion that GS-ddR emanates, in part, from the AP sites formed from the glycosylase-mediated repair of alkylated nucleobase lesions.

Influence of APE1 Inhibition on the Generation of GS-ddR.

Mammalian AP-endonuclease APE1 was shown to be capable of removing the 3′-PUA generated from the β-elimination of the AP site.[66,67] APE1 may also trim GS-ddR to produce a 3′-hydroxyl terminus for polymerase β-mediated gap filling,[51] and the endonuclease activity of APE1 on AP sites precludes the generation of GS-ddR. We used the APE1 inhibitor CRT0044867 to examine the influence of APE1 inhibition on the generation of GS-ddR. Consistent with the aforementioned findings, incubation with 100 μM MNU for 1 h elicited an increased level of GS-ddR in HEK293T cells (Figure 5A). Treatment with the APE1 inhibitor led to further elevation in the GS-ddR level, suggesting that APE1 could trim this type of modified 3′-terminus within cells. APE1 inhibition, however, did not influence the background level of GS-ddR in HEK293T cells (Figure 5A), which is consistent with the previous finding that the background level of 3′-PUA in the DNA of mouse embryonic stem cells was not perturbed upon APE1 inhibition.[21] As expected, the level of MNU-induced O^6-MedG was not impacted by APE1 inhibition (Figure 5B). Hence, these results revealed that APE1 inhibition could augment the level of GS-ddR in MNU-treated cells. This could be attributed to APE1's direct function in trimming of 3′-GS-ddR or its indirect role in minimizing GS-ddR formation, that is, through the removal of AP sites, thereby reducing cellular levels of 3′-PUA, the precursor for GS-ddR formation.

CONCLUSIONS

In summary, we developed an LC–MS/MS combined with the stable-isotope dilution method for sensitive and accurate quantification of GS-ddR in the DNA of cultured human cells. By employing this method, we found that the basal level of GS-ddR in HEK293T cells is 2–5 lesions per 10^7 nucleosides. We also applied the method to investigate the time- and dose-dependent induction of GS-ddR by MNU and the influence of APE1 on MNU-induced formation of GS-ddR. Our results showed that MNU treatment stimulated a dose-dependent induction of GS-ddR and O^6-MedG within cells, and the repair of GS-ddR trails that of O^6-MedG. The latter is consistent with the notion that GS-ddR arises partly from the AP sites formed from the repair of alkylated nucleobase lesions. Moreover, our results also revealed a role of APE1 in modulating the GS-ddR level in human cells.

Supplementary Material

Refer to Web version on PubMed Central for supplementary material.

ACKNOWLEDGMENTS

This work was supported by the National Institutes of Health (R01 ES021007 to K.S.G. and Y.W.).

REFERENCES

(1). Lindahl T Nature 1993, 362, 709–715. [PubMed: 8469282]
(2). Lindahl T Angew. Chem., Int. Ed 2016, 55, 8528–8534.
(3). De Bont R; van Larebeke N Mutagenesis 2004, 19, 169–185. [PubMed: 15123782]
(4). Nakamura J; Walker VE; Upton PB; Chiang S-Y; Kow YW; Swenberg JA Cancer Res. 1998, 58, 222–225. [PubMed: 9443396]

(5). Wang Z; Chandrasena ER; Yuan Y; Peng K-W; van Breemen RB; Thatcher GRJ; Bolton JL Chem. Res. Toxicol 2010, 23, 1365–1373. [PubMed: 20509668]

(6). Rusyn I; Asakura S; Li Y; Kosyk O; Koc H; Nakamura J; Upton PB; Swenberg JA DNA Repair 2005, 4, 1099–1110. [PubMed: 16051529]

(7). Park J-H; Troxel AB; Harvey RG; Penning TM Chem. Res. Toxicol 2006, 19, 719–728. [PubMed: 16696575]

(8). Viswesh V; Gates K; Sun D Chem. Res. Toxicol 2010, 23, 99–107. [PubMed: 20017514]

(9). Gates KS The chemical reactions of DNA damage and degradation. In Reviews of Reactive Intermediate Chemistry, 2007; 333–378.

(10). Lindahl T; Karlstrom O Biochemistry 1973, 12, 5151–5154. [PubMed: 4600811]

(11). Lindahl T; Nyberg B Biochemistry 1972, 11, 3610–3618. [PubMed: 4626532]

(12). Lindahl T Prog. Nucleic Acid Res. Mol. Biol 1979, 22, 135–192. [PubMed: 392601]

(13). David SS; Williams SD Chem. Rev 1998, 98, 1221–1262. [PubMed: 11848931]

(14). Thompson PS; Cortez D DNA Repair 2020, 90, No. 102866. [PubMed: 32417669]

(15). Loeb LA; Preston BD Annu. Rev. Genet 1986, 20, 201–230. [PubMed: 3545059]

(16). Jackson AL; Loeb LA Mutat. Res., Fundam. Mol. Mech. Mutagen 2001, 477, 7–21.

(17). Barnes DE; Lindahl T Annu. Rev. Genet 2004, 38, 445–476. [PubMed: 15568983]

(18). Lindahl T; Andersson A Biochemistry 1972, 11, 3618–3623. [PubMed: 4559796]

(19). Gates KS Chem. Res. Toxicol 2009, 22, 1747–1760. [PubMed: 19757819]

(20). Hegde ML; Hazra TK; Mitra S Cell Res. 2008, 18, 27–47. [PubMed: 18166975]

(21). Rahimoff R; Kosmatchev O; Kirchner A; Pfaffeneder T; Spada F; Brantl V; Müller M; Carell TJ Am. Chem. Soc 2017, 139, 10359–10364.

(22). Guillet M; Boiteux S EMBO J. 2002, 21, 2833–2841. [PubMed: 12032096]

(23). Haldar T; Jha JS; Yang Z; Nel C; Housh K; Cassidy OJ; Gates KS Chem. Res. Toxicol 2022, 35, 218–232. [PubMed: 35129338]

(24). Böhme A; Thaens D; Schramm F; Paschke A; Schürmann G Chem. Res. Toxicol 2010, 23, 1905–1912. [PubMed: 20923215]

(25). Bricteux-Grégoire S; Verly WG Nucleic Acids Res. 1989, 17, 6269–6282. [PubMed: 2475855]

(26). Bricteux-Grégoire S; Verly WG Biochem. J 1991, 273, 777–782. [PubMed: 1705116]

(27). Dutta S; Chowdhury G; Gates KS J. Am. Chem. Soc 2007, 129, 1852–1853. [PubMed: 17253689]

(28). Price NE; Johnson KM; Wang J; Fekry MI; Wang Y; Gates KS J. Am. Chem. Soc 2014, 136, 3483–3490. [PubMed: 24506784]

(29). Varela JG; Pierce LE; Guo X; Price NE; Johnson KM; Yang Z; Wang Y; Gates KS Chem. Res. Toxicol 2021, 34, 1124–1132. [PubMed: 33784065]

(30). Yang Z; Price NE; Johnson KM; Wang Y; Gates KS Nucleic Acids Res. 2017, 45, 6275–6283. [PubMed: 28531327]

(31). Housh K; Jha JS; Yang Z; Haldar T; Johnson KM; Yin J; Wang Y; Gates KS J. Am. Chem. Soc 2021, 143, 15344–15357. [PubMed: 34516735]

(32). Sczepanski JT; Zhou C; Greenberg MM Biochemistry 2013, 52, 2157–2164. [PubMed: 23480734]

(33). Mohni KN; Wessel SR; Zhao R; Wojciechowski AC; Luzwick JW; Layden H; Eichman BF; Thompson PS; Mehta KPM; Cortez D Cell 2019, 176, 144–153.e13. [PubMed: 30554877]

(34). Thompson PS; Amidon KM; Mohni KN; Cortez D; Eichman BF Nat. Struct. Mol. Biol 2019, 26, 613–618. [PubMed: 31235915]

(35). Chan W; Ham Y-H; Jin L; Chan HW; Wong Y-L; Chan C-K; Chung P-Y Anal. Chem 2019, 91, 4987–4994. [PubMed: 30896925]

(36). Chan W; Jin L Anal. Chem 2022, 94, 803–810. [PubMed: 34971314]

(37). Male R; Fosse VM; Kleppe K Nucleic Acids Res. 1982, 10, 6305–6318. [PubMed: 6294597]

(38). Minko IG; Jacobs AC; de Leon AR; Gruppi F; Donley N; Harris TM; Rizzo CJ; McCullough AK; Lloyd RS Sci. Rep 2016, 6, 28894. [PubMed: 27363485]

(39). Piersen CE; McCullough AK; Lloyd RS DNA Repair 2000, 459, 43–53.
(40). McCullough AK; Sanchez A; Dodson ML; Marapaka P; Taylor J-S; Lloyd RS Biochemistry 2001, 40, 561–568. [PubMed: 11148051]
(41). Wyatt MD; Pittman DL Chem. Res. Toxicol 2006, 19, 1580–1594. [PubMed: 17173371]
(42). Kondo N; Takahashi A; Ono K; Ohnishi TJ Nucleic Acids 2010, 2010, No. 543531.
(43). Fu D; Calvo JA; Samson LD Nat. Rev. Cancer 2012, 12, 04–120.
(44). Lehmann F; Wennerberg J Process 2021, 9, 377.
(45). Menke M; Meister A; Schubert I Mutagenesis 2000, 15, 503–506. [PubMed: 11077002]
(46). Shrivastav N; Li D; Essigmann JM Carcinogenesis 2010, 31, 59–70. [PubMed: 19875697]
(47). Loveless A Nature 1969, 223, 206–207. [PubMed: 5791738]
(48). Hickman MJ; Samson LD Mol. Cell 2004, 14, 105–116. [PubMed: 15068807]
(49). Klapacz J; Meira LB; Luchetti DG; Calvo JA; Bronson RT; Edelmann W; Samson LD Proc. Natl. Acad. Sci. U. S. A 2009, 106, 576–581. [PubMed: 19124772]
(50). Gates KS; Nooner T; Dutta S Chem. Res. Toxicol 2004, 17, 839–856. [PubMed: 15257608]
(51). Jha JS; Yin J; Haldar T; Yang Z; Wang Y; Gates KS J. Am. Chem. Soc 2022, 144, 10471–10482. [PubMed: 35612610]
(52). Meister A; Anderson ME Annu. Rev. Biochem 1983, 52, 711–760. [PubMed: 6137189]
(53). Bellomo G; Vairetti M; Stivala L; Mirabelli F; Richelmi P; Orrenius S Proc. Natl. Acad. Sci. U. S. A 1992, 89, 4412–4416. [PubMed: 1584774]
(54). Wang J; Yuan B; Guerrero C; Bahde R; Gupta S; Wang Y Anal. Chem 2011, 83, 2201–2209. [PubMed: 21323344]
(55). Liu L; Taverna P; Whitacre CM; Chatterjee S; Gerson SL Clin. Cancer Res 1999, 5, 2908–2917. [PubMed: 10537360]
(56). Pezuk AJ; Valera TE; Delsin EAL; Scrideli AC; Tone GL; Brassesco SM Cent. Nerv. Syst. Agents Med. Chem 2016, 16, 67–72.
(57). Eads JR; Krishnamurthi SS; Saltzman J; Bokar JA; Savvides P; Meropol NJ; Gibbons J; Koon H; Sharma N; Rogers L; Pink JJ; Xu Y; Beumer JH; Riendeau J; Fu P; Gerson SL; Dowlati A Invest. New Drugs 2021, 39, 142–151. [PubMed: 32556884]
(58). Talpaert-Borlé M; Liuzzi M Biochim. Biophys. Acta, Gene Struct. Expression 1983, 740, 410–416.
(59). Zhou X; Liberman RG; Skipper PL; Margolin Y; Tannenbaum SR; Dedon PC Anal. Biochem 2005, 343, 84–92. [PubMed: 15964542]
(60). Wei S; Shalhout S; Ahn Y-H; Bhagwat AS DNA Repair 2015, 27, 9–18. [PubMed: 25616257]
(61). Wang Y; Liu L; Wu C; Bulgar A; Somoza E; Zhu W; Gerson SL Nucl. Med. Biol 2009, 36, 975–983. [PubMed: 19875055]
(62). Chen H; Yao L; Brown C; Rizzo CJ; Turesky RJ Anal. Chem 2019, 91, 7403–7410. [PubMed: 31055913]
(63). Hong H; Cao H; Wang Y; Wang Y Chem. Res. Toxicol 2006, 19, 614–621. [PubMed: 16696563]
(64). An R; Jia Y; Wan B; Zhang Y; Dong P; Li J; Liang X PLoS One 2015, 9, No. e115950.
(65). Yu Y; Wang J; Wang P; Wang Y Anal. Chem 2016, 88, 8036–8042. [PubMed: 27441891]
(66). Marenstein DR; Chan MK; Altamirano A; Basu AK; Boorstein RJ; Cunningham RP; Teebor GW J. Biol. Chem 2003, 278, 9005–9012. [PubMed: 12519758]
(67). Pascucci B; Maga G; Hübscher U; Bjoras M; Seeberg E; Hickson ID; Villani G; Giordano C; Cellai L; Dogliotti E Nucleic Acids Res. 2002, 30, 2124–2130. [PubMed: 12000832]

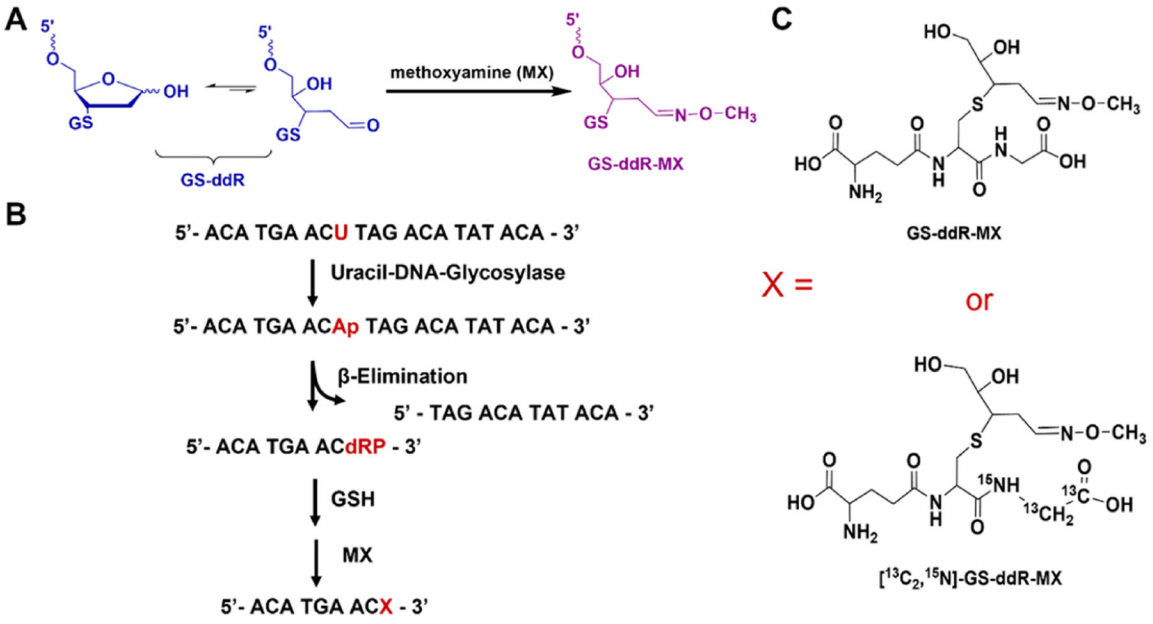

Figure 1.

Generation of GS-ddR-MX-containing ODNs. (A) Scheme illustrating the reaction between the aldehyde terminus of GS-ddR and methoxyamine (MX). (B) Schematic diagram depicting the procedures for the generation of a GS-ddR-MX-containing ODN from a single-stranded uracil-containing ODN. (C) Chemical structures of GS-ddR-MX and [$^{13}C_2$, ^{15}N]-GS-ddR-MX.

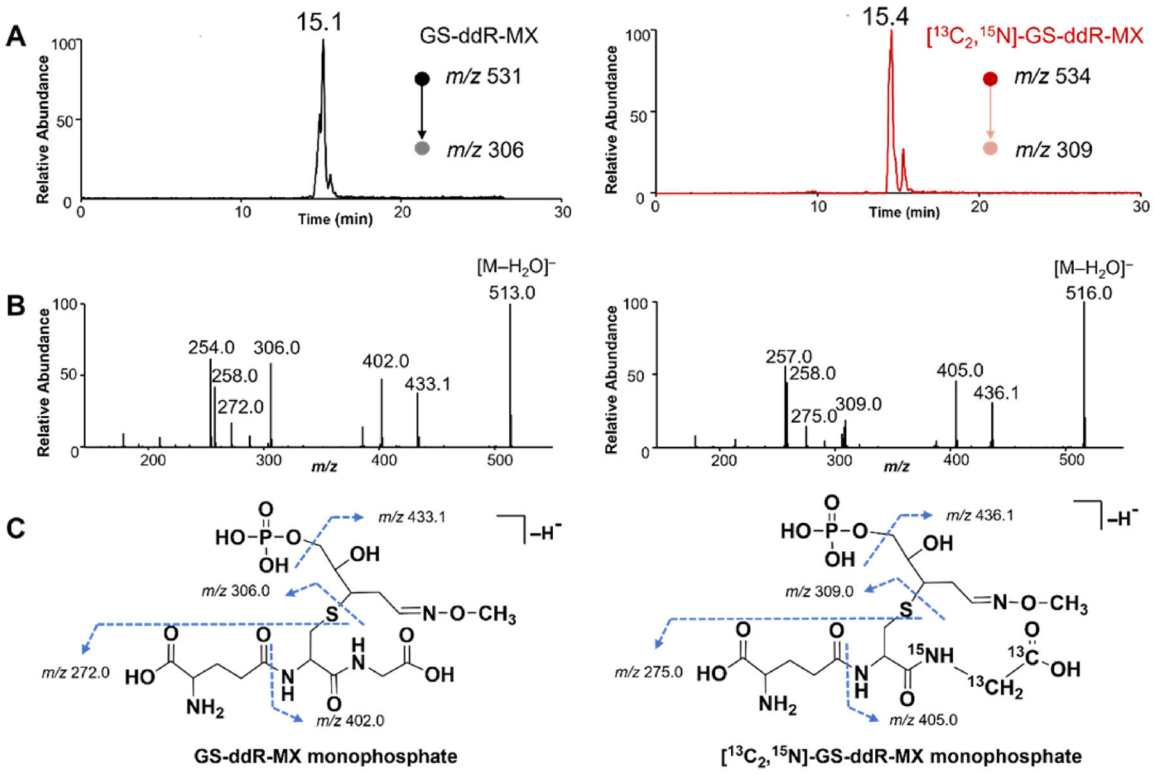

Figure 2.

LC–MS/MS characterizations of GS-ddR-MX monophosphate in the negative-ion mode. (A) Representative SICs for monitoring the *m*/*z* 531 → 306 and 534 → 309 transitions for the $[M - H]^-$ ions of GS-ddR-MX and [$^{13}C_2$, ^{15}N]-GS-ddR-MX monophosphates, respectively, in the nuclease P1 digestion mixtures of the corresponding ODNs. (B) Negative-ion ESI-MS/MS of GS-ddR-MX (left) and [$^{13}C_2$, ^{15}N]-GS-ddR-MX (right) monophosphates. (C) Proposed fragmentation patterns of product ions observed in the MS/MS of the $[M - H]^-$ ions of GS-ddR-MX (left) and [$^{13}C_2$, ^{15}N]-GS-ddR-MX (right) monophosphates.

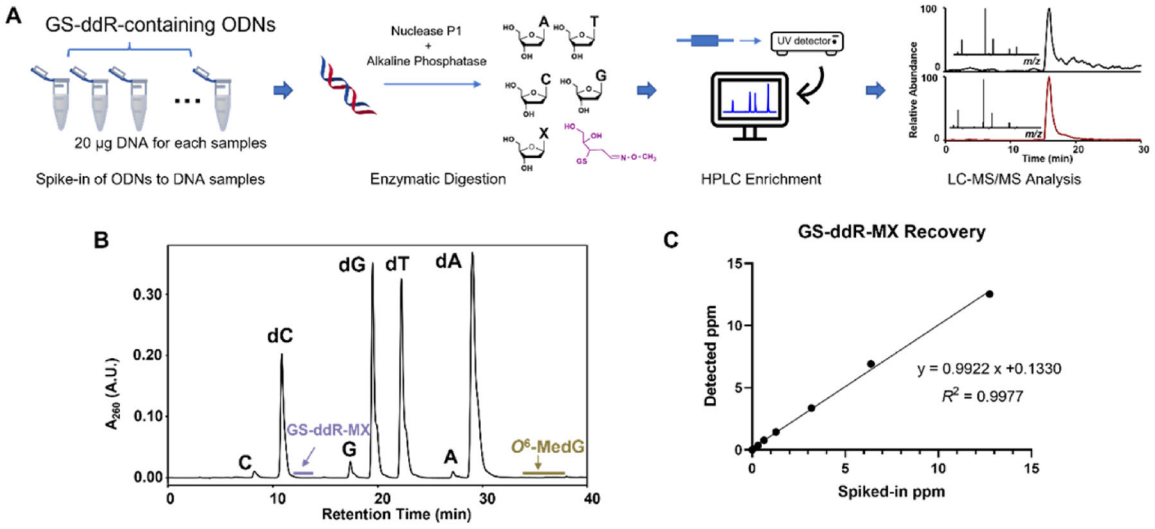

Figure 3.

Recovery of GS-ddR-MX from the lesion-containing ODNs. (A) Workflow of sample preparation for the LC–MS/MS analysis of GS-ddR-MX in DNA samples. “X” in the “Enzymatic Digestion” part represents modified nucleobases. (B) Representative HPLC trace for the enrichment of GS-ddR-MX and O^6-MedG from the nucleoside digestion mixture of DNA samples isolated from HEK293T cells treated with MNU. (C) Recovery calibration curve of GS-ddR-MX obtained from LC–MS/MS analyses of the enzymatic digestion mixtures of calf thymus DNA spiked with different amounts of a GS-ddR-MX-containing ODN and a fixed amount (20 fmol) of [$^{13}C_2$, ^{15}N]-GS-ddR-MX-containing ODN, which was used as the internal standard. Plotted are the detected versus spiked-in levels of GS-ddR in calf thymus DNA.

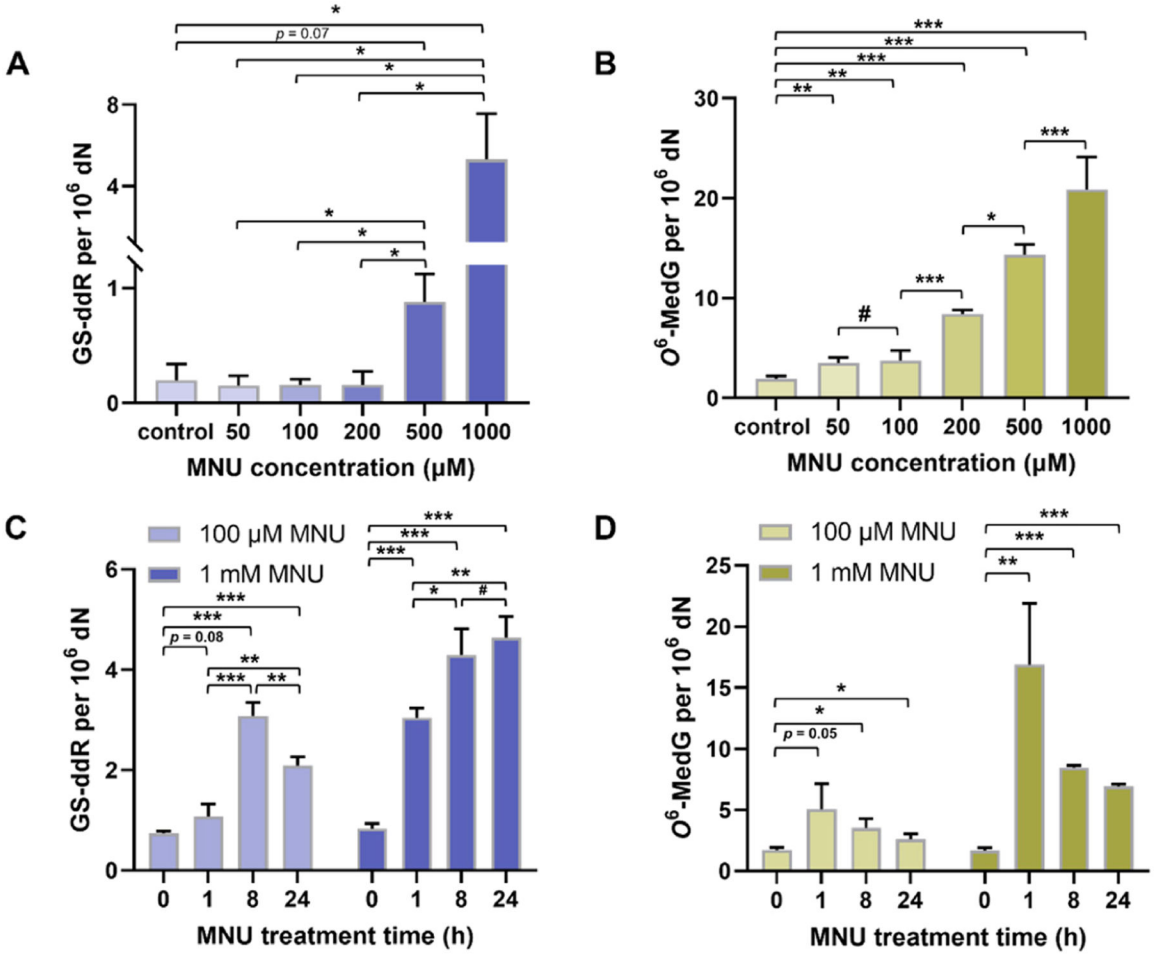

Figure 4.

Time- and dose-dependent induction of GS-ddR in HEK293T cells treated with MNU. (A,B) Quantification results for the levels of GS-ddR (A) and O^6-MedG (B) in HEK293T cells treated with 0, 50, 100, 200, 500 μM, and 1 mM of MNU for 1 h. p-values were calculated by using Kruskal–Wallis one-way ANOVA and Conover's multiple comparisons test further adjusted by the Benjamini–Hochberg FDR method for the comparison between control and MNU treatments with different concentrations and the comparison between different concentration treatments. (C,D) Quantification results for the levels of GS-ddR (C) and O^6-MedG(D) in HEK293T cells treated with 100 μM or 1 mM of MNU for 0, 1, 8, and 24 h. The data in (A–D) represent the mean ± S.D. ($n = 3$) of results from three independent experiments. The results for GS-ddR and O^6-MedG were acquired by LC–MS/MS analysis on a QE Plus quadrupole-Orbitrap and an LTQ XL linear ion trap mass spectrometer, respectively. The p values were calculated by using the unpaired two-tailed t test for the comparison between 0 h and different treatment times and the comparison between different treatment times. #, $p > 0.05$; *, $0.01 < p < 0.05$; **, $0.001 < p < 0.01$; ***, $p < 0.001$.

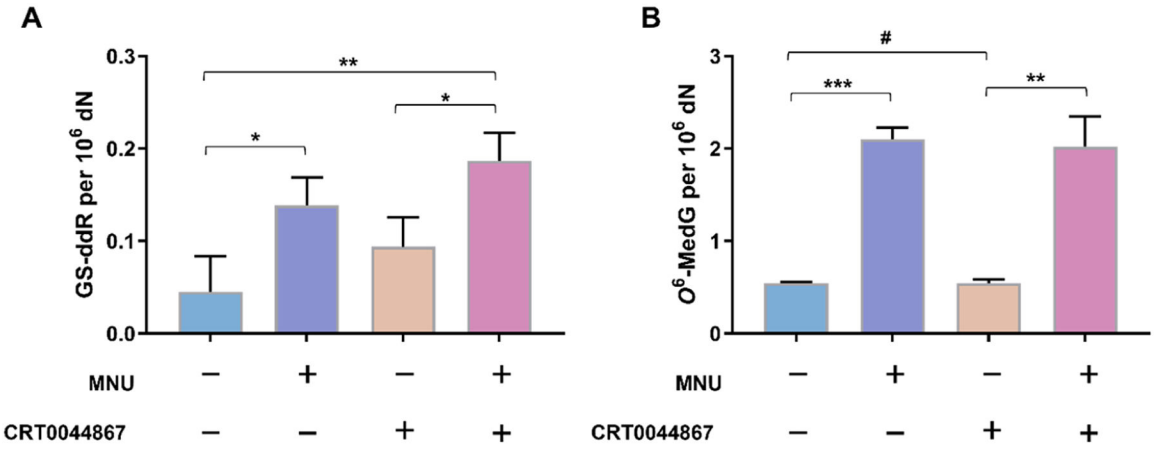

Figure 5.

Effects of APE1 inhibition on the generation of GS-ddR. (A,B) Quantification results for the levels of GS-ddR (A) and O^6-MedG (B) in the HEK293T cells treated with MNU, APE1 inhibitor (CRT0044867), alone or in combination. The data represent mean ± S.D. ($n = 3$) of results from three independent experiments. The p values were calculated by using the unpaired two-tailed t test (#, $p > 0.05$; *, $0.01 < p < 0.05$; **, $0.001 < p < 0.01$; ***, $p < 0.001$).

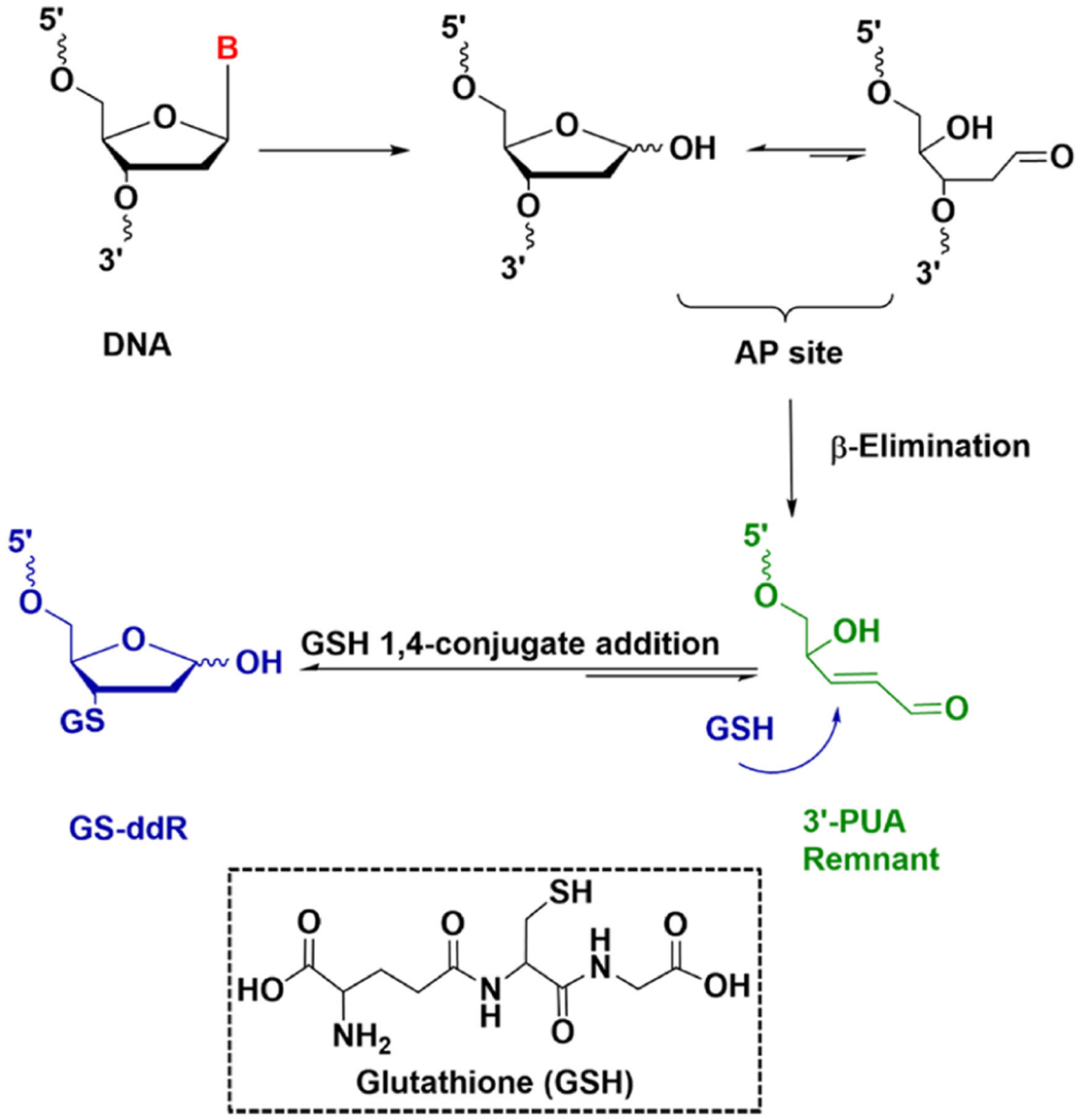

Scheme 1.

GS-ddR Arising from the Strand Cleavage at an AP Site in the Presence of Glutathione

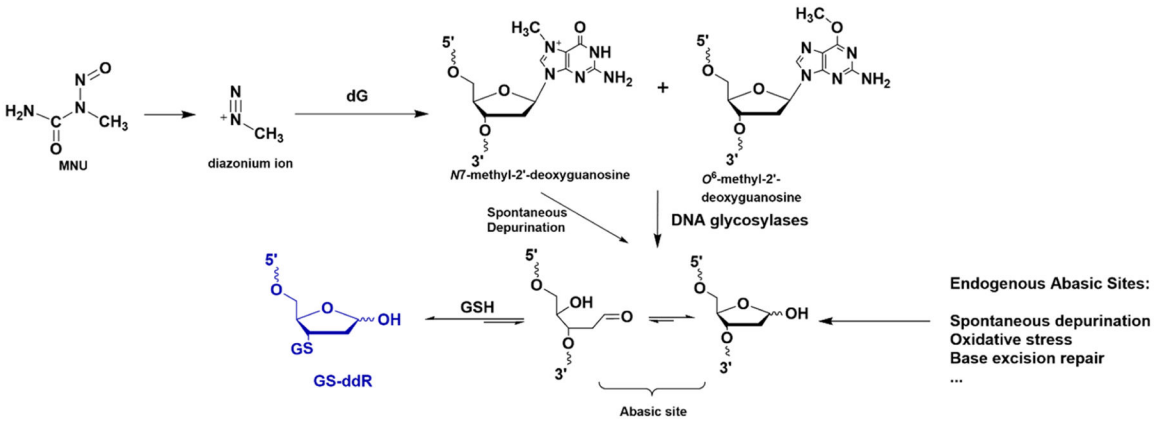

Scheme 2.

MNU-Induced Generation of *N*7-Methyl-2′-deoxyguanosine and O^6-Methyl-2′-deoxyguanosine and the Subsequent Formation of GS-ddR